Optical properties of a small-particle composite

K. D. Cummings,* J. C. Garland, and D. B. Tanner†
Department of Physics, Ohio State University, Columbus, Ohio 43210
(Received 3 August 1983; revised manuscript received 30 July 1984)

Room-temperature reflectance measurements over frequencies between the far infrared and the ultraviolet have been made on composites of silver small particles and potassium chloride grains. The optical properties of these composites were obtained by Kramers-Kronig analysis. Comparison of the data with the Maxwell-Garnett theory and the effective-medium approximation showed that the effective-medium approximation better described the data. A sum-rule analysis indicates that the expected linear relationship between the volume fraction of metal and the integrated oscillator strength is obeyed.

I. INTRODUCTION

This paper describes the optical properties of a three-dimensional composite consisting of silver (Ag) and potassium chloride (KCl) small particles. This composite serves as a model system for the study of randomly inhomogeneous media. The strength of the inhomogeneity is large because the electronic properties of the highly conducting Ag particles and of the insulating KCl grains are quite different. Depending on the amount of metal present in the composite, the optical properties can display either metallic or insulating behavior.

Relatively few attempts have been made to correlate the optical properties of a composite with those of the constituent parts, despite the importance of inhomogeneous materials. Four types of composite have been employed in previous studies. First, a number of optical transmission measurements have been made on dielectric substances containing very small amounts of conducting particles.[1–5] In these cases, sample characterization was difficult because the metal particles were generally grown *in situ*. Second, discontinuous films[6–14] and granular metal films (cermets)[15–21] have received a considerable amount of attention. These systems have the advantage of being easy to produce over wide ranges of metal concentration. Their drawbacks are that the grains of these films are correlated (as shown by the very high volume fraction of metal necessary for percolation), that they are two dimensional, and that the insulating component is often not well characterized. Third, optical measurements on free-standing metal particles produced by gas evaporation have been made.[22–25] Sample control and characterization in this system is easily obtained and the samples can be made sufficiently thick to be clearly three dimensional. However, the particles are correlated (stuck together), and therefore do not represent a particularly random system.

The fourth type of sample—the composite system chosen in this work—alleviates many of the problems discussed above. The volume fraction of metal in this sample can be varied from 0 to nearly 1. The small Ag particles can be made nearly uniform in size[26,27] and can be embedded in the KCl to produce a three-dimensional sample that is more random than other types of systems.

The next section of this paper describes sample preparation and optical techniques while the third section presents our reflectance data and the results of a Kramers-Kronig analysis. In the final section we discuss comparisons of our data with theories of inhomogeneous media and evaluate a number of sum rules.

II. EXPERIMENTAL TECHNIQUE

A. Ag-particle production

The Ag metal particles were made by evaporation in a noble-gas—oxygen atmosphere. This technique, which has been used to produce "smokes" or blacks from such metals as Au, Al, Ag, and Sn, produces single crystalline, nearly spherical small particles with a relatively narrow size distribution.[26,27] We evaporated Ag metal from an aluminum-oxide-coated molybdenum boat in an ordinary evaporator through which a mixture of 75 vol % argon and 25 vol % oxygen was flowed at a rate of approximately 35 cm^3/min. The pressure in the bell jar was stabilized to 1 Torr by adjusting the pumping speed. Both the pressure and the temperature (current through the boat) were kept constant until all of the Ag had been evaporated from the boat. The particles were collected on a clean glass cylinder, placed around the boat, as black smoke. In the evaporation process the Ag vapor loses energy to the noble-gas atoms, causing the Ag to cool and coalesce into small particles. The oxygen was introduced into the apparatus to produce a thin oxide coating on the metal particles. This coating prevented the Ag particles from cold-welding together during evaporation but apparently was sufficiently thin to allow metal-to-metal contact between the particles under sufficient pressure.[28] After the silver had been evaporated, the smoke was collected from the glass and its resistance measured. Only smokes with a resistance greater than 1 MΩ were used to make the composite samples.

An electron micrograph of the smoke is shown in Fig. 1. The particles appear to be spherical with average radius of 120 Å and follow a log-normal size distribution[26] with a geometric standard deviation of about 1.5. Using

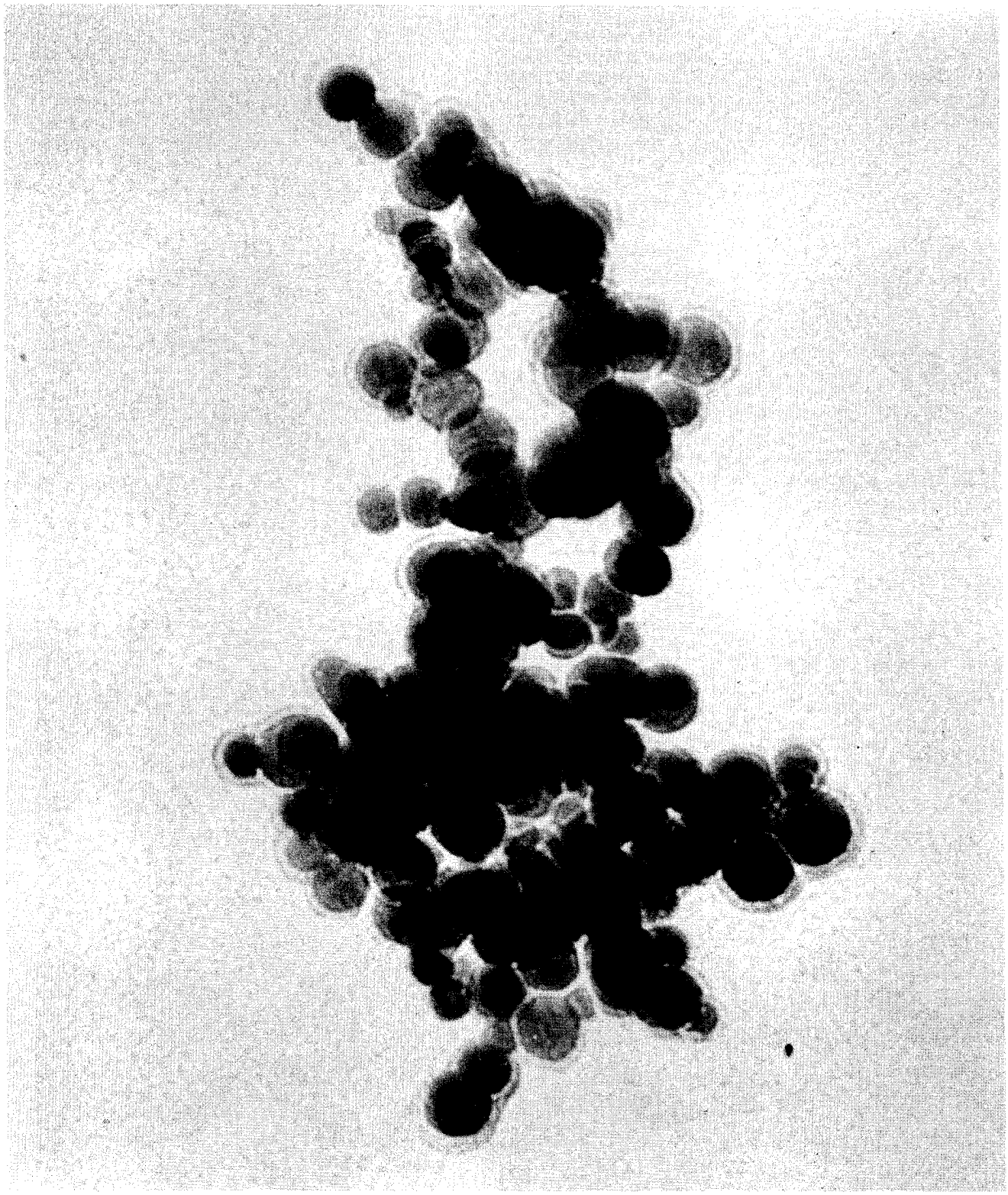

FIG. 1. Transmission electron micrograph of the Ag particles used in the samples. The average particle diameter is 250 Å.

the procedure described in the preceding paragraph, we were able consistently to convert 80% of the Ag into smoke which had a mean diameter of 250 Å and a measured resistance greater than 1 MΩ.

B. Composite manufacture

The composite samples were created by mixing the Ag smoke with powdered KCl with use of a cyclical prepara-

tion procedure. The total amount of KCl necessary for a sample was weighed out and sufficient Ag powder was added to this KCl to make the volume fraction f of Ag 0.01. The powders were mixed and then compressed (9 kbar) in an evacuated (1 mTorr) die to make a wafer-shaped sample. The pressure was sufficient to fracture the KCl particles and fuse them together, effectively filling the voids in the loosely packed mixture.[27] The wafer was broken into small fragments to which more Ag was added. This new mixture was ground at liquid-nitrogen temperature in a SPEX Freezer/Mill and repressed under vacuum into another wafer. This stepwise increase of volume fraction allowed the Ag to mix uniformly with the KCl. The volume fraction was increased in 0.01 steps for $0<f<0.05$, in 0.05 steps until 0.05 below the desired value, and in 0.01 steps to the final volume fraction. The mixing process was completed by grinding and pressing four more times. The wafer was ground a fifth time after

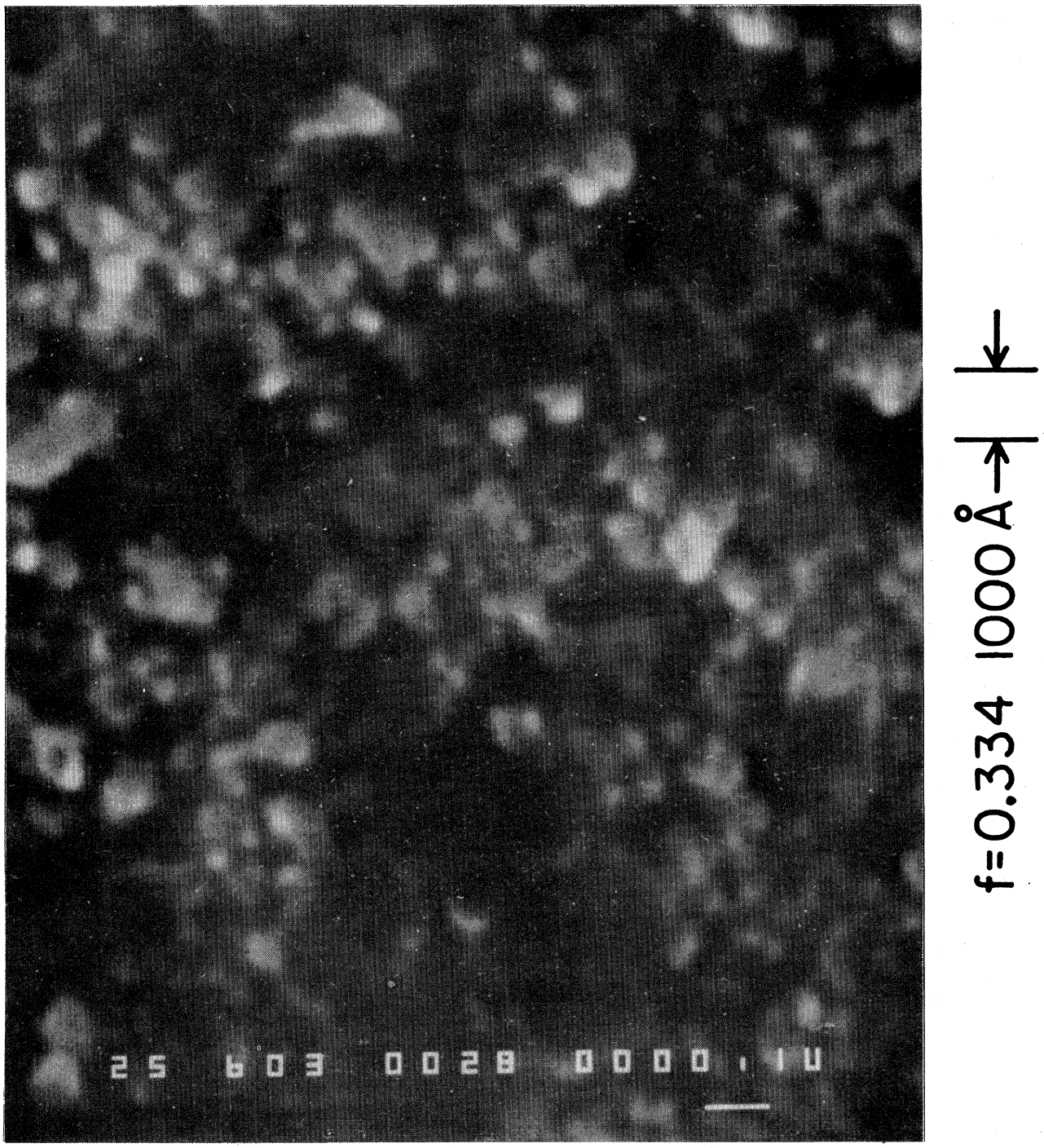

FIG. 2. High magnification scanning electron micrograph of the Ag particles at the surface of a $f=0.334$ composite sample. The particles are the round white objects in this photograph.

which the powder was baked in a vacuum oven at 150 °C to remove water vapor, which the KCl had absorbed during the mixing process. The final sample was made by removing the powder from the oven and pressing a 0.6-cm-diam. pellet approximately 0.3 cm thick.

To obtain accurate reflection measurements of the samples, the surface had to be smooth and flat. The pellet was epoxied onto the end of a threaded rod, ground flat with 600-grit emery paper, and polished using 5-, 1-, and 0.3-μm alumina powders. The samples were wetted with isopropanol throughout the polishing process. With the use of this procedure most samples could be made flat and quite shiny in appearance.

Despite this appearance the samples showed some effects of diffuse scattering, which increased as the sample surfaces were attacked by atmospheric water vapor. Particularly at high frequencies, the rough surface caused the reflectance to be smaller than it should have been. In an attempt to compensate for this scattering, the samples were coated with 3000 Å of Au immediately after the re-

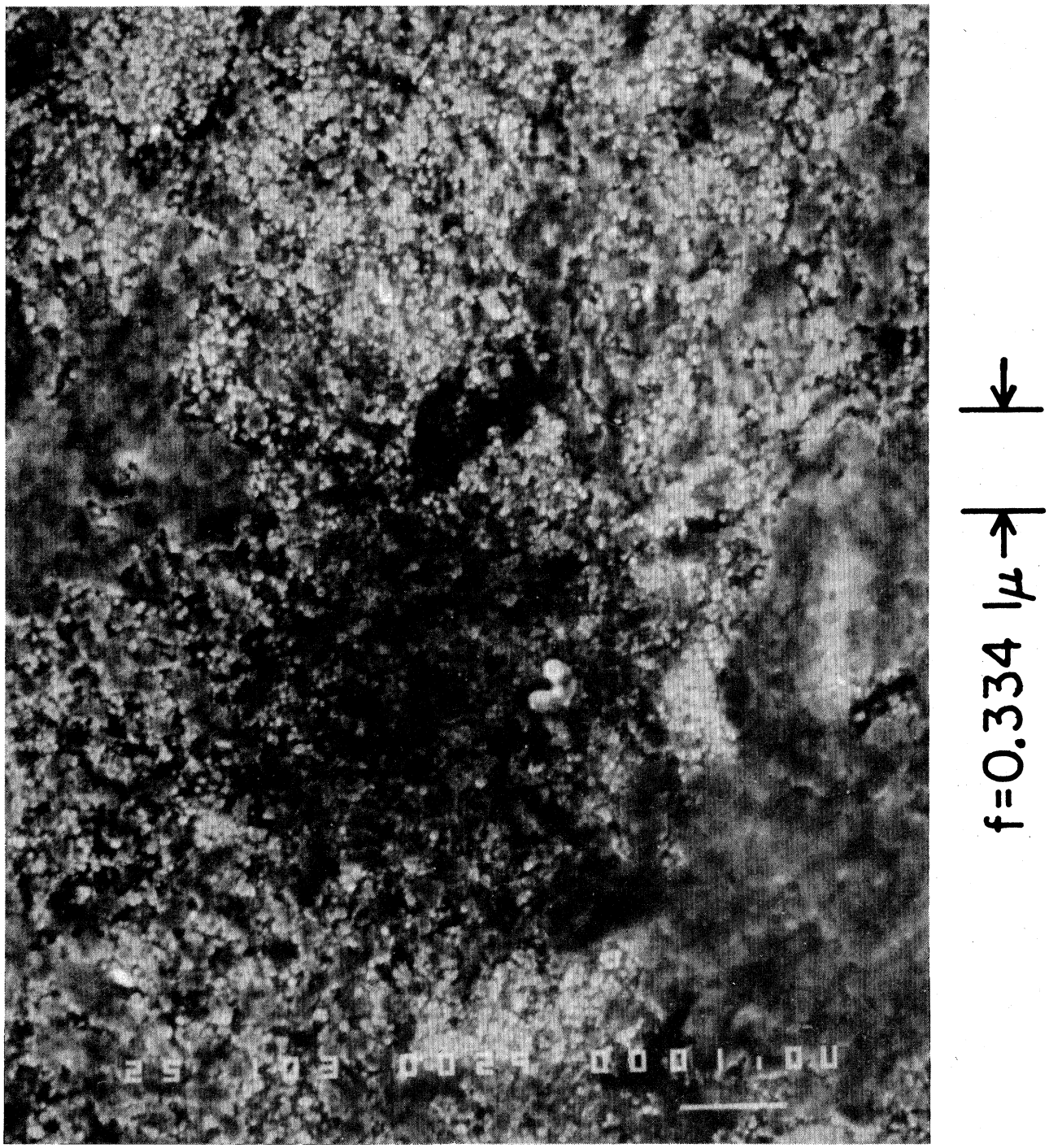

FIG. 3. Scanning electron micrograph of the sample surface at moderate magnification. The particles are the small white dots.

flectance was measured. A comparison between the gold-coated surface and the uncoated surface gave a correction of the reflection spectrum for scattering.

C. Characterization in electron microscope

We used a JEOL JXA-35 electron probe x-ray microanalyzer (scanning electron microscope) for structural and chemical characterization of the composite samples. Figure 2 shows an example of the Ag particles at the surface of a composite having $f=0.334$. Comparison with Fig. 1 shows that the particles retain their spherical appearance during the pressing and grinding process. Figure 3 is a lower-magnification view, showing the distribution of the Ag particles at the surface of the sample. The small white dots are the Ag particles. Notice that the particles are not isolated into large islands but instead are distributed across the entire surface of the sample.[29]

To determine quantitatively the amounts of the elements present in the samples, x-ray elemental analysis was performed in the scanning electron microscope using an EDAX 9100 system. X-rays, generated when the electron beam strikes the sample, are energy analyzed; from the intensity of the characteristic x-ray emission the atomic percent of each element can be calculated. Quantitative analysis was accomplished using a modified version of FRAME-C, a National Bureau of Standards program developed for energy-dispersive x-ray analysis, to correct inter-elemental effects.

The analysis of the composites gave the atomic percent of the major components (Ag, K, and Cl). However, the analysis also indicated that many samples had sulfur (S) contamination on the Ag particles. Ag tarnishes by reacting with atmospheric sulfur compounds to form Ag_2S. The Ag volume fraction (f) of each sample was calculated from the atomic percent concentration (N_{Ag}) by assuming bulk densities for each constituent after correcting for the S contamination by assuming that each S atom bonded to 2 Ag atoms and removed these "free" electrons from the metallic part of the sample. The volume fraction is

$$f=\frac{(N_{Ag}-2N_S)M_{Ag}}{\rho_{Ag}V}\ , \tag{1}$$

where N_S is the atomic concentration of sulfur, M_{Ag} is the atomic mass of silver, ρ_{Ag} is the bulk density of Ag, and V is the total sample volume. N_S/N_{Ag} varied from nearly zero to 11%; its average value was 5%.

Another element that existed in the composites was the oxygen (O) introduced to produce the oxide coating on the particles. The EDAX system is completely insensitive to O, so that the x-ray analysis probably indicated more free Ag metal then was truly present. Previous work[26] with Ag particles produced in an argon and oxygen atmosphere indicates the oxide coating could be about 10 Å thick. This coating could reduce the volume fraction of free Ag by about 20%. However, care was taken in the Ag particle manufacture consistently to produce similar amounts of oxide on all particles. Note that whereas Ag tarnishes while stored at room temperature, we would not expect it to oxidize. In addition, sum-rule calculations, discussed in Sec. IV, indicate that for the majority of the samples the oxide coating reduces f by only small amounts.

D. Evidence for randomness

We believe that the location of the metal grains in our sample is reasonably random. There are three reasons for this belief. First, the electron microscope, both in its imaging and in its x-ray mapping mode, showed no large-scale (>1 μm) clumping of the Ag grains in the samples prepared as described above. In the case of samples which were pressed only once the x-ray mapping did show regions of high Ag concentration, but after the fifth press no clumping could be discerned. Second, the samples undergo a percolation transition at a critical concentration which is very close to the expected value[30,31] of 0.16—0.18. Previous dielectric constant measurements,[27] which used the mass of the Ag powder to determine the concentration, found $f_c^m=0.20\pm0.01$. Our electron-microscope characterization showed that the concentration is systematically overestimated when the mass is used, so that a corrected value of f_c is $f_c=0.17\pm0.01$, in very good agreement with theory. Third, a detailed study of the stepwise sample manufacturing process finds[32] that the electrical resistance of a sample is initially increased when the sample is ground up and repressed (without adding more Ag!). After five to six cycles of grinding and pressing, the resistance increase stops. Similarly, the dielectric constant of low-concentration samples increased during the first few cycles but stabilized by the fifth step in the process. Our interpretation of this experiment is that initially the Ag particles, which at $r=120$ Å are smaller than the approximately 1-μm-size KCl grains, are not randomly located but instead fill the gaps between KCl. Upon regrinding, the KCl fractures along new planes, leaving some Ag in the interior of the grains. With the cyclical procedure the Ag eventually has an opportunity to be located anywhere within the composite. If this behavior did not occur, the resistance should not be affected by the grinding and pressing cycle.

E. Reflectance measurements

A Michelson interferometer and 1-K bolometer detector were used to measure the reflectance in the 10-to-700—cm^{-1} (1-to-90—meV) region.[33,34] With beam-splitters of 2.5 and 12 μm thickness the reflectance was examined with a resolution of $\Delta\omega/\omega=10^{-2}$.

A vacuum spectrometer, built around a Perkin-Elmer model 16 U grating monochromator,[33] was used to measure the reflectance in the 500-to-45 000—cm^{-1} (0.06-to-5.6—eV) region. Three sources, four gratings, and three detectors were used to cover the infrared, visible, and ultraviolet regions with moderate resolution, $\Delta\omega/\omega=10^{-3}$.

III. EXPERIMENTAL RESULTS

A. Reflectance

Figure 4 shows the reflectance of several samples. Notice that the low-frequency reflectance increases with increasing volume fraction of Ag and that the plasma

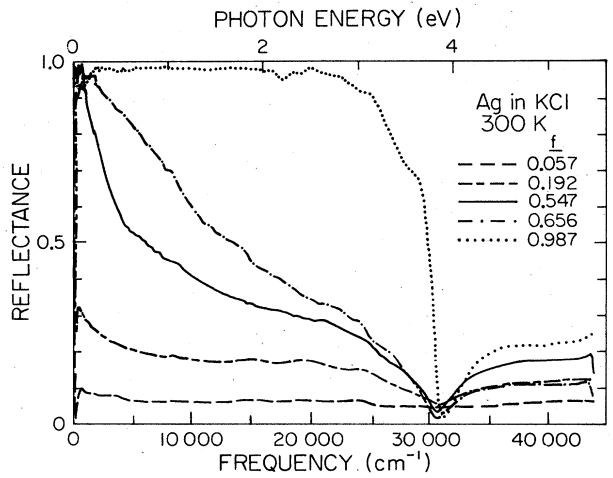

FIG. 4. Reflectance between 10 and 45 000 cm^{-1} (1 meV to 5.6 eV) of room-temperature Ag-KCl composites for several volume fractions.

minimum of Ag (at 31 500 cm^{-1} or 3.9 eV) is apparent in all the samples. The sharp rise in the reflectance after the plasma minimum is due to interband transitions of electrons in Ag.[35] The Ag film that was used for the $f=0.987$ sample has structure at 29 500 cm^{-1} (3.7 eV). The structure has been identified as a surface plasmon which was excited in the Ag film.[36] Figure 5 shows the low-frequency behavior of several samples. The structure at 150 cm^{-1} (10 meV) is due to optic phonons in KCl.[37] This structure disappears as the volume fraction of Ag is increased.

B. Kramers-Kronig transformation

Because the reflectance measurements covered an extremely large frequency range (10—45 000 cm^{-1}), a Kramers-Kronig analysis of the reflectance provides accurate values for the optical constants. The Kramers-Kronig integral determines the phase shift on reflection.[38] With the measured reflectance and the phase shift known, any optical function can be calculated.

Conventional extrapolation procedures were used in the Kramers-Kronig analysis. Samples having low dc conductivity were assumed to have a constant reflectance between zero frequency and 10 cm^{-1}. This approximation assumes the lowest data points are a good estimate of the dc value of the reflectance. The reflectance of samples with large dc conductivities was assumed to follow at low frequencies the Hagen-Reubens relation,[39]

$$R(\omega)=1-A\omega^{1/2}\,, \tag{2}$$

where R is the reflectance as a function of frequency and A was chosen to make the relation fit the first few data points. This approximation is valid for the low-frequency reflectance of metals so long as the dc conductivity (in esu units) is much greater than the frequency. For Ag the dc conductivity is approximately 10^6 times larger than the lowest frequency, making this approximation valid for our conducting samples.

A second extrapolation was done for frequencies between the last data point (45 000 cm^{-1} or 5.6 eV) and 400 000 cm^{-1} (50 eV). Here, the reflectance was extrapolated as ω^{-s}, with the exponent chosen to be $s=0.8$, a value consistent with the behavior[40] of bulk Ag between 50 000 and 400 000 cm^{-1}. Above 400 000 cm^{-1} the reflectance was assumed to follow a ω^{-4} form, as appropriate for free-electron behavior.

To permit comparison with dc properties, we have calculated from the Kramers-Kronig analysis the frequency-dependent conductivity $\sigma_1(\omega)$ and the real part of the dielectric function $\epsilon_1(\omega)$. Together these quantities determine the complex dielectric function:

$$\epsilon(\omega)=\epsilon_1(\omega)+\frac{4\pi i}{\omega}\sigma_1(\omega)\,. \tag{3}$$

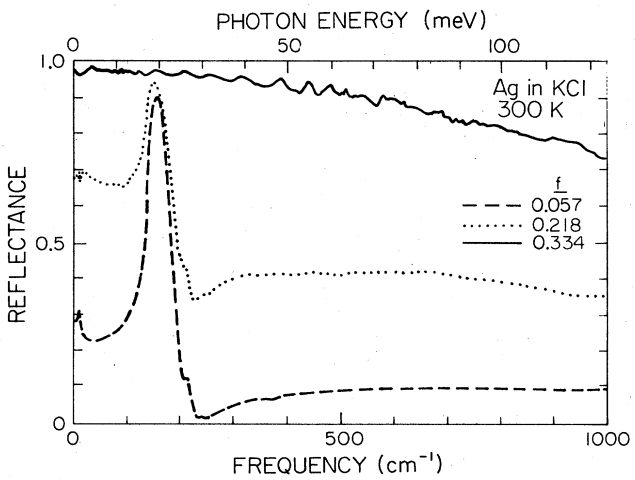

FIG. 5. Reflectance data showing low-frequency (10—1000 cm^{-1} or 1—125 meV) detail. Structure at 150 cm^{-1} (10 meV) is from the transverse-optic mode of KCl.

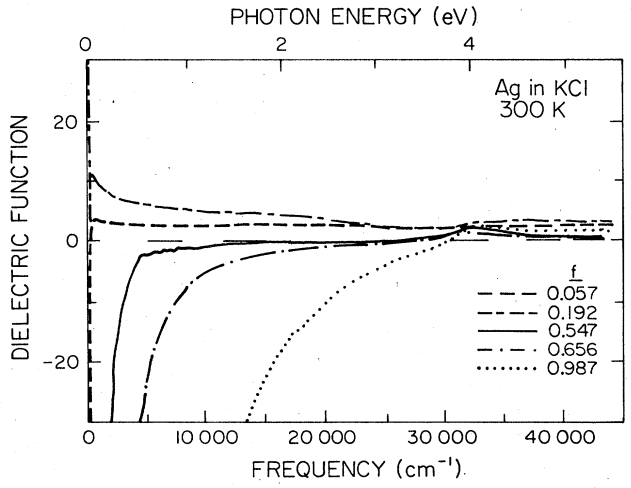

FIG. 6. Real part of the dielectric function obtained by Kramers-Kronig analysis of the reflectance of Ag-KCl composites.

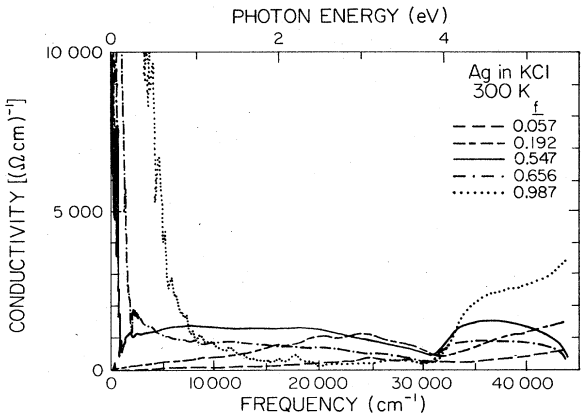

FIG. 7. Frequency-dependent conductivity obtained by Kramers-Kronig analysis of the reflectance of Ag-KCl composites.

C. Dielectric function

Figure 6 shows the real part of the dielectric function, ϵ_1, as determined by the Kramers-Kronig analysis. Notice that the low-frequency values of ϵ_1 are positive for low-volume fractions and negative for higher-volume fractions. The change in low-frequency behavior is caused by the insulator to metal (percolation) transition in our system. The sharp decrease at low frequencies is from the free electrons which give Ag metal a high reflectivity and conductivity in the infrared. Measurements[27] of the static dielectric constant indicate the percolation transition occurs at a volume fraction very close to that of the $f=0.192$ sample. The structure in ϵ_1 at 32 000 cm^{-1} is from the electrons of the d states,[35] which lie 4 eV below the Fermi surface in Ag.

D. Conductivity

Figure 7 shows the Kramers-Kronig result for the frequency-dependent conductivity, $\sigma_1(\omega)$. There is a minimum in the conductivity just above 3000 cm^{-1} (4 eV) followed by a sharp rise in the conductivity at the onset of the interband transitions. Notice the large change in the low-frequency values of the conductivity as the volume fraction of Ag increases. Figure 8 shows the low-frequency conductivity for three low-concentration samples in detail. (Note that for samples with $f>0.3$, the conductivity in this frequency range is off scale.) The peak at 140 cm^{-1} is from the transverse-optic phonon[37] of KCl. The strength of this peak actually increases with increasing volume fraction of metal. As we shall see, this effect is predicted by the theories of composite materials.[41] At higher concentrations ($f>0.3$) we no longer see the optic phonon.

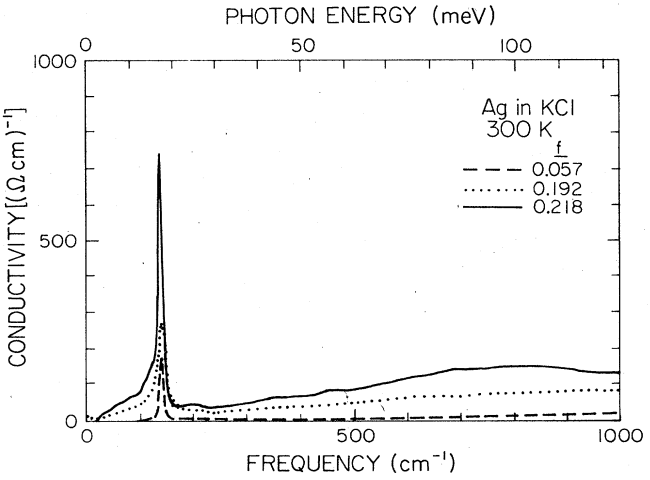

FIG. 8. Frequency-dependent conductivity showing low-frequency detail.

IV. DISCUSSION

A. The effective dielectric function

In our samples, where the scale over which spatial fluctuations occur (particle size) is small compared to the wavelength of the incident electromagnetic fields, the inhomogeneous medium may be viewed as being uniform in its response to external fields. The optical properties[42–55] of this medium are described by an effective homogeneous dielectric function, which depends on the dielectric function of Ag, the dielectric function of KCl, the volume fraction of metal (f), the particle size, and the particle shape. We will assume a spherical shape for the particles in our treatment. There exist two different theories for the effective dielectric function,[42] the Maxwell-Garnett theory (MGT) and the effective-medium approximation (EMA).

According to the MGT,[43] isolated grains of dielectric function ϵ_Q are embedded in a host material with dielectric function ϵ_H. No contact between the grains is permitted in this theory. These assumptions, which correspond to low-volume fraction f, lead to the MGT dielectric function:

$$\epsilon_{\mathrm{MGT}}=\epsilon_H+\frac{3\epsilon_H f(\epsilon_G-\epsilon_H)}{(1-f)(\epsilon_G-\epsilon_H)+3\epsilon_H} . \tag{4}$$

Note that Eq. (4) is inherently asymmetric in the treatment of the two constituents, giving different answers for the case of metal grains embedded in an insulating background and for insulating grains in a metal background, even if the volume fraction of metal is the same in both cases. In addition, ϵ_{MGT} varies smoothly from the host value at $f=0$ to the grain value at $f=1$; i.e., there is no percolation transition.[44–47] Such a transition is specifically excluded by the assumption that the metal grains make no contact. Despite these shortcomings, the MGT has been applied to numerous metal-insulator composite systems[6,8,10,11,14,15,18,24,48,54,55] and is generally accepted as a good description of dilute inhomogeneous mixtures.

According to the EMA,[49] individual grains, either metal or insulator, are considered to be embedded in a background (the "effective medium"), which has the average properties of the mixture. A self-consistent choice for the properties of the effective medium leads to a quadratic equation for the dielectric function of the medium ϵ_{EMA},

$$f\frac{\epsilon_M-\epsilon_{\rm EMA}}{\epsilon_M+2\epsilon_{\rm EMA}}+(1-f)\frac{\epsilon_I-\epsilon_{\rm EMA}}{\epsilon_I+2\epsilon_{\rm EMA}}=0\ . \tag{5}$$

Equation (5) displays the symmetrical treatment of the materials within the EMA, remaining unchanged if the insulating and metallic grains are interchanged while keeping the volume fraction of metal the same (i.e., $f\rightarrow 1-f$). The EMA allows for a percolation transition,[46,50–52] at a critical volume fraction $f_c=\frac{1}{3}$ for spherical particles. Like the MGT, the EMA has been applied to numerous systems and has been generalized to optical frequencies by many investigators.[21,46,51–54]

It has been pointed out that in addition to the electric dipole effects which lead to Eqs. (4) and (5), small metal particles also interact with the magnetic part of the external field.[48,53–58] We have incorporated this eddy-current effect in our calculations, but find that it is not very important at the concentrations and frequencies which we have studied.

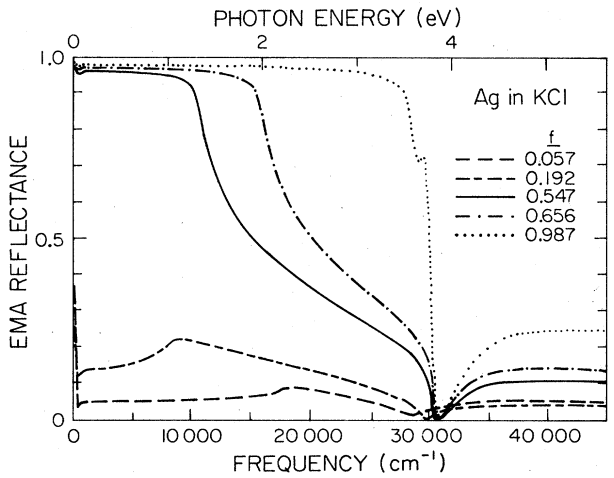

FIG. 9. Reflectance of Ag-KCl composites as calculated by the effective-medium approximation.

B. Properties of Ag and KCl

We have used semiclassical models for the dielectric response of KCl and Ag in the MGT and EMA. KCl is a diatomic crystal with a fundamental lattice vibration in the far infrared. We choose a Lorentz oscillator model[38] to represent this transverse-optic-phonon mode[37] in the dielectric function of KCl ($\epsilon_{\rm KCl}$)

$$\epsilon_{\rm KCl}(\omega)=\epsilon_{\rm opt}+\frac{\omega_L^2}{\omega_{\rm TO}^2-\omega^2-i\gamma\omega}\ . \tag{6}$$

In Eq. (6), $\epsilon_{\rm opt}=2.1$ is the high-frequency value of the dielectric function for KCl; $\omega_{\rm TO}=141$ cm^{-1} is the resonance frequency of the vibrational mode of the ions;[39] ω_L^2 describes the oscillator strength for the phonon; and $\gamma=5$ cm^{-1} is the full width at half maximum for the oscillator. The oscillator strength ω_L^2 was calculated by the relation[39]

$$\omega_L^2=\epsilon_{\rm opt}(\omega_{\rm LO}^2-\omega_{\rm TO}^2)\ , \tag{7}$$

where $\omega_{\rm LO}=200$ cm^{-1} is the longitudinal polariton frequency, defined to be the zero of the real part of dielectric function. This relation gives $\omega_L=206$ cm^{-1}.

Ag is a metal with d bands beginning 4 eV below the Fermi energy.[35] Therefore below 4 eV only intraband transitions of electrons occur, whereas above 4 eV interband transitions also occur. The dielectric function of Ag ($\epsilon_{\rm Ag}$) can be represented as a combination of a free-electron Drude model[38,39] for low-frequency behavior and tabular data[40] for the higher-frequency bound-particle behavior:

$$\epsilon_{\rm Ag}(\omega)=\epsilon_b(\omega)-\frac{\omega_p^2}{\omega^2+i\omega/\tau}\ . \tag{8}$$

Here, $\epsilon_b(\omega)$ describes the interband and core electron contributions to the dielectric function of bulk Ag, taken from Ref. 40. The other quantities in Eq. (8) are $\omega_p=73\,100$ cm^{-1}, the unscreened plasma frequency[35] for the conduction electrons, and τ, the electronic relaxation time. Because the Ag particles are small ($r=125$ Å), the relaxation time is dominated by surface collisions even at room temperature. To account for this scattering, we add a term to the relations rate ($1/\tau=v_F/l$) that assumes electrons, traveling at the Fermi velocity (v_F) in a particle of radius r, scatter diffusely from the particle surface,

$$1/\tau=1/\tau_{\rm Ag}+v_F/r\ . \tag{9}$$

Using the scattering rate[36] of bulk Ag (for which $l=300$ Å), we calculate $1/\tau=740$ cm^{-1} for our 120-Å-radius Ag particles. (Note that in converting from sec^{-1} to cm^{-1}, one divides by $2\pi c$.)

C. Band structure of small particles

As mentioned above, Ag is a metal with d bands lying approximately 4 eV (32 000 cm^{-1}) below the Fermi energy.[35] Figures 4 and 7 show d interband transitions in our composites; both the reflectance and conductivity rise above 30 000 cm^{-1}. The appearance of these interband transitions at the same energy as in the bulk metal shows that the electronic structure of our small (120-Å-radius)

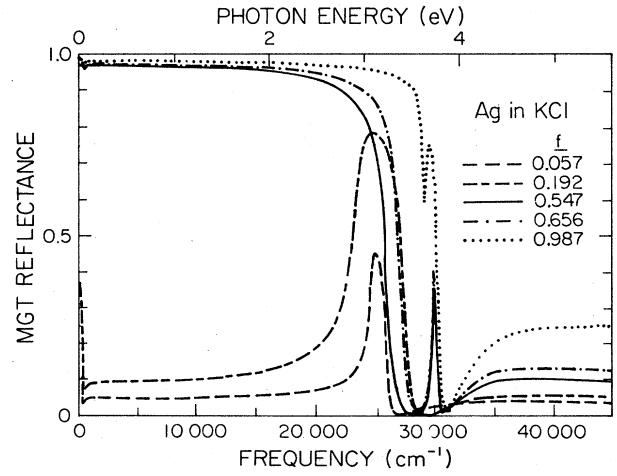

FIG. 10. Reflectance of Ag-KCl composites as calculated by the Maxwell-Garnett theory.

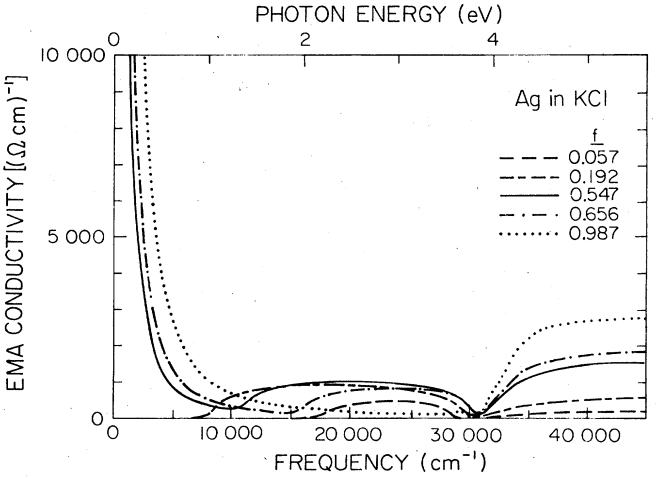

FIG. 11. Conductivity of Ag-KCl composites as calculated by the effective-medium approximation.

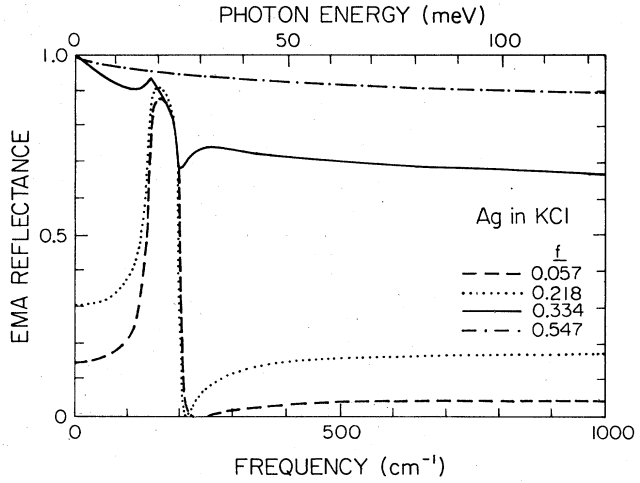

FIG. 13. Effective-medium—approximation calculation of the reflectance showing low-frequency detail.

particles is similar to the bulk.

Ideally the magnitude of $\sigma_1(\omega)$ above 4 eV should change systematically with f. This is the case over 30 000–37 000 cm^{-1}, except for the $f=0.656$ sample. We attribute this failure to an imperfect correction for the diffuse scattering from our samples.

D. Comparison between data and theories

Figures 9 and 10 show the calculated reflectance with use of the EMA and MGT. To obtain reasonable results from the MGT, samples with $f<0.5$ were assumed to consist of Ag particles in a KCl host, whereas those with $f>0.5$ had KCl grains in an Ag host. This switch from an insulating host to a conducting host artificially produces a percolation transition at $f=0.5$ in the MGT calculations. In contrast, the percolation transition occurs automatically in the EMA when $f=\frac{1}{3}$. A comparison of Fig. 4 with Figs. 9 and 10 shows that the EMA correctly predicts the rising low-frequency reflectance and the increasing sharpness of the 3.9-eV plasma minimum with increasing volume fraction of Ag, whereas the MGT predicts a sharp resonance at 3.1 eV (KCl host) and 3.7 eV (Ag host) that is not seen in our data.

The frequency-dependent conductivity also supports the conclusion that the EMA better describes our samples. A comparison of the calculated conductivity, Figs. 11 and 12, with the data, Fig. 7, shows that the EMA correctly predicts a broad peak in the conductivity with a maximum value of $\sim 1000\ \Omega^{-1}cm^{-1}$. The sharp peaks predicted by the MGT at 3.1 eV (KCl host) or 3.7 eV (Ag host) are not seen in our data.

E. Low-frequency properties

Figure 13 shows the EMA calculation of low-frequency reflectance, showing the disappearance of the transverse-optic phonon of KCl with increased volume fraction of

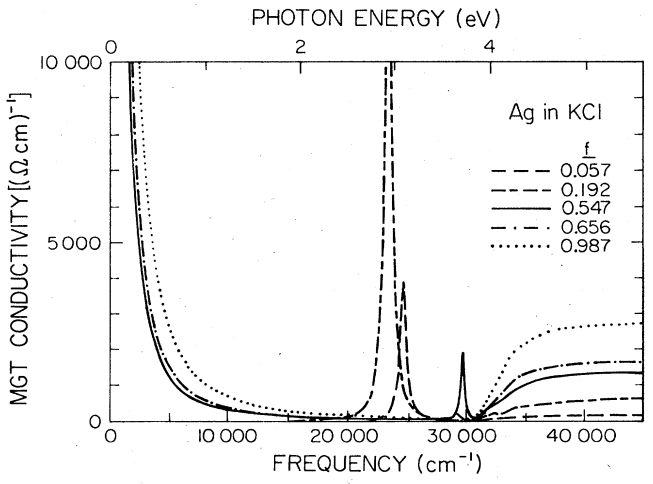

FIG. 12. Conductivity of Ag-KCl composites as calculated by the Maxwell-Garnett theory.

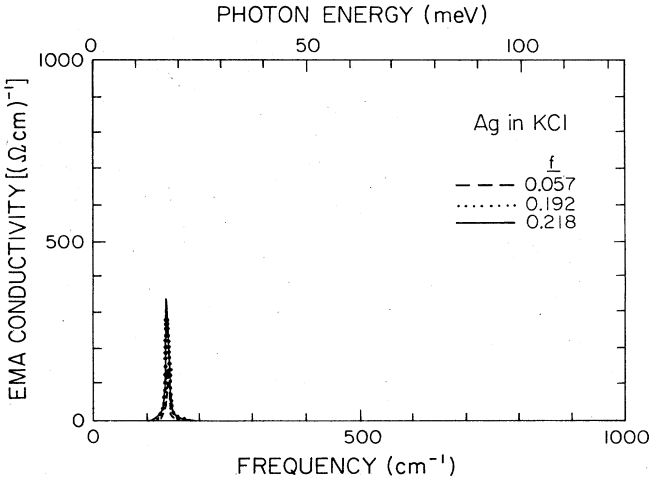

FIG. 14. Effective-medium—approximation calculation of the conductivity showing low-frequency detail.

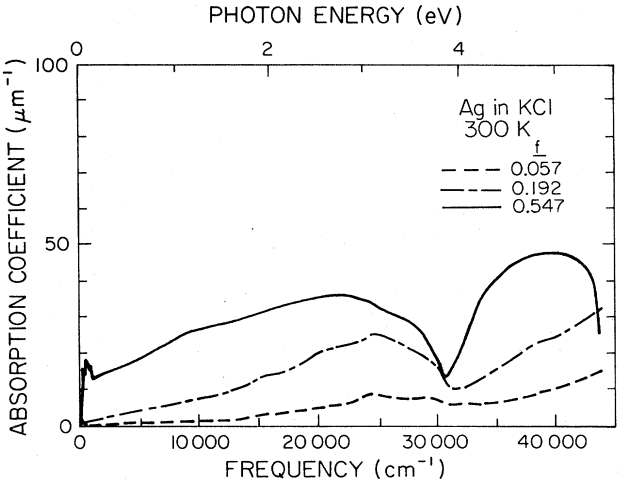

FIG. 15. Absorption coefficient obtained by Kramers-Kronig analysis of the room-temperature reflectance. 1 μm^{-1} equals 10 000 cm^{-1}.

metal. Note that as in the experimental results (Fig. 5) the phonon mode disappears just above the percolation transition ($f \approx 0.2$ in our samples and $f = \frac{1}{3}$ in the EMA). In the EMA calculation of $\sigma_1(\omega)$ at low frequency shown in Fig. 14, the transverse-optic mode of KCl is seen to be enhanced with increasing volume fraction. The magnitude of the phonon peak is in reasonable agreement with experiment (Fig. 8) for $f < f_c \approx 0.2$. Thus, the EMA and experiment agree well in the low-frequency region so long as both are either above or below their critical volume fractions. Note that at these frequencies the KCl-host MGT is similar to the EMA for $f < \frac{1}{3}$, whereas the Ag-host MGT is similar to the EMA for $f > \frac{1}{3}$.

F. Absorption coefficient

Figure 15 shows the absorption coefficient for some of our samples. Previous work[48,54,59] has shown that the absorption coefficient $\alpha(\omega)$ of an inhomogeneous medium to be

$$\alpha(\omega) = (2\omega/c)\,\mathrm{Im}(\epsilon_M \mu_M)^{1/2}\,, \tag{10}$$

where c is the speed of light, ϵ_M is the dielectric function of the medium, and μ_M is its permeability. At low frequencies and small volume fraction $\alpha(\omega)$ can be written as[48,59]

$$\alpha(\omega) = K f \omega^{\beta}\,, \tag{11}$$

where K depends, according to theory,[48] upon the particle radius and dc conductivity. At low values of f and ω, $\beta = 2$. As f and ω are increased, β is expected to decrease to a value less than 1. This qualitative behavior is seen in our data.

G. Sum rules

Stroud[60] has derived several sum rules for composite systems. Using our model for Ag and neglecting any small contributions from the KCl, we are able to rewrite the optical conductivity sum rule as a partial sum rule for the Ag-KCl composites:

$$(2m/\pi n e^2) \int_0^{\omega_c} \sigma_1(\omega)\,d\omega = f N_e m/m^*\,, \tag{12}$$

where m is the free-electron mass, e the electronic charge, n the atomic number density for Ag, N_e the number of conduction electrons per Ag atom, σ_1 the real part of the conductivity, ω the angular frequency, ω_c the cutoff frequency for the partial sum, and $N_e m/m^*$ is the oscillator strength. From the free-electron model for Ag we expect $N_e m/m^*$ to rise rapidly at low frequencies and saturate at a value near 1, the number of valence-conduction electrons per Ag atom. Thus, the left-hand side of Eq. (12) should equal f. Figure 16 shows the result of evaluating

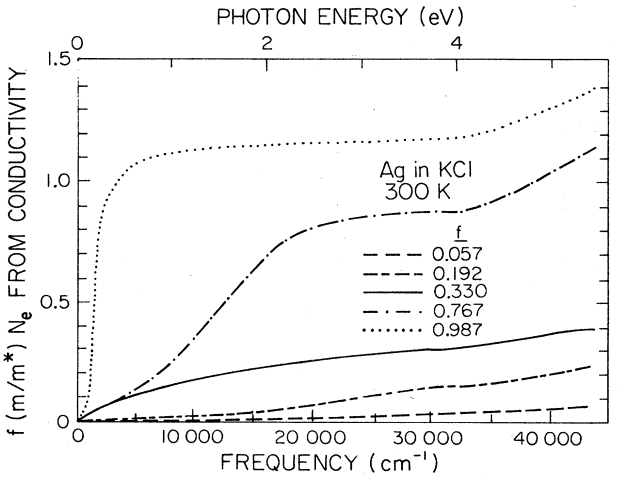

FIG. 16. The partial oscillator strength versus frequency, determined by integration of the Kramers-Kronig derived conductivity.

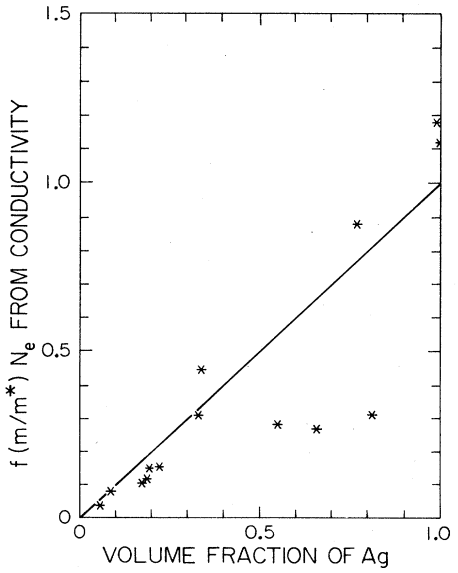

FIG. 17. Intraband oscillator strength vs volume fraction from conductivity data. The line is the expected result for our system.

Eq. (12) for our samples. For Ag, $f=0.987$, there is a broad plateau between the regions of free-electron behavior and interband transitions. For the other samples, the saturation occurs at higher frequencies and at lower values of the oscillator strengths.

To enable comparison of all our samples, we evaluated the partial sum rule at the plasma minimum of bulk Ag ($\omega_c = 31\,500$ cm^{-1} or 3.9 eV) and assumed that the oscillator strength of bulk Ag at this frequency was $N_e m/m^* = 1$. Equation (12) predicts a linear relationship between the volume fraction and oscillator strength. Figure 17 shows the calculated oscillator strength versus volume fraction; the line is the expected result. Notice that the simple assumptions of this model are not quite correct. The value for bulk Ag is slightly higher than one.[37] This increased oscillator strength probably comes from a small interband contribution at ω_c. Many of the samples give values that fit the expected results very well. Three higher-concentration samples, however, are much lower than expected. This discrepancy probably occurs because the surfaces of these samples were not polished sufficiently well.

We may write two more sum rules that relate optical response functions to the oscillator strength of the composites. They are

$$(mc/2\pi^2 ne^2)\int_0^{\omega_c}\alpha(\omega)d\omega = fN_e m/m^* , \quad (13)$$

$$-(m/2\pi^2 ne^2)\int_0^{\omega_c}\omega\,\mathrm{Im}[1/\epsilon(\omega)]d\omega = fN_e m/m^* , \quad (14)$$

where α is the absorption coefficient, $-\mathrm{Im}(1/\epsilon)$ is the loss function,[38] and c is the speed of light. Figures 18 and 19 give, respectively, the evaluation of Eqs. (13) and (14) versus volume fraction; the lines are the expected result scaled by the value[40] for bulk Ag. The absorption coefficient sum rule is satisfied rather well. In contrast, the loss function sum rule [Eq. (14)] fails to describe our data. This failure occurs mainly because of the very low values of the loss function sum rule. We expect the data would fit the predicted results better if the integration could be carried to much higher frequencies.

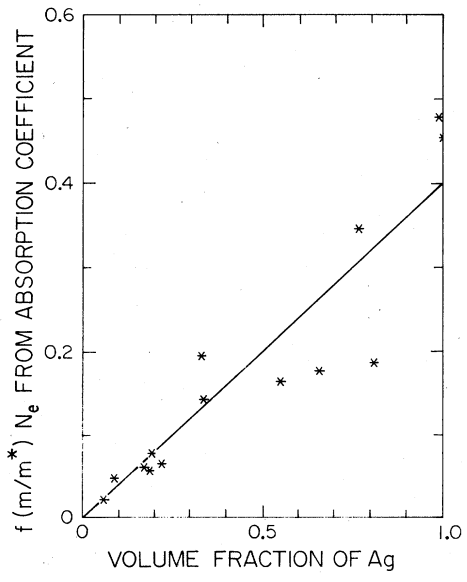

FIG. 18. Intraband oscillator strength vs volume fraction from absorption coefficient data. The line is the expected result for our system.

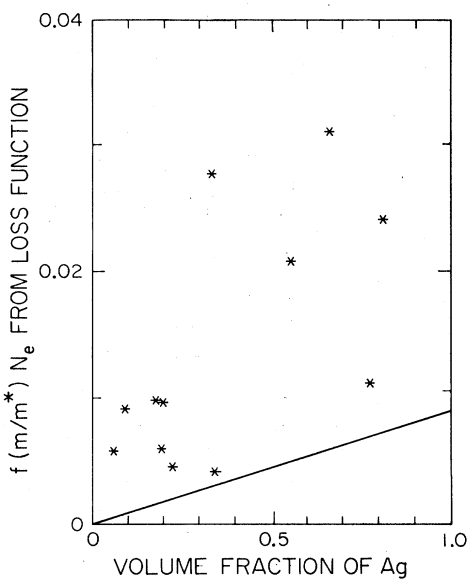

FIG. 19. Intraband oscillator strength vs volume fraction from loss function data. The line is the expected result for our system.

Stroud[60] also derived a sum rule for the second moment of the conductivity. Again using our model for the composite his expression may be written as a partial sum rule

$$(3m^2/2\pi^2 n^2 e^4)\int_0^{\omega_c}\omega^2\sigma_1(\omega)d\omega = f(1-f) , \quad (15)$$

where f is the volume fraction of Ag. We now use Eq. (15) and (12) to obtain additional information about the broad peak in the data, shown in Fig. 7 at around 25 000 cm^{-1} (3 eV), and in the EMA, shown in Fig. 13 at approximately 20 000 cm^{-1} (2.5 eV). This peak arises from absorption by standing-wave modes excited in the small metal particles by the incident electromagnetic radiation and is called the "impurity band" by Stroud. The square of the center of gravity for the impurity band in the composites can be calculated by dividing the integral in Eq. (15) by the integral in Eq. (12) to give

$$\omega_{\mathrm{imp}}^2 = \left[\int_0^{\omega_c}\omega^2\sigma_1(\omega)d\omega\right] \Big/ \left[\int_0^{\omega_c}\sigma_1(\omega)d\omega\right] . \quad (16)$$

The "center of gravity" of the band (ω_{imp}) is the location the band would have if it had zero width. Note that above percolation, the center of gravity is a weighted average of the "percolation mode" at zero frequency and the impurity band. Figure 20 plots the ratio of the center frequency of the impurity band to the plasma frequency, $\omega_{\mathrm{imp}}/\omega_p$, versus the volume fraction of Ag. The line is the expected result for spherically symmetric composites below percolation as described by Stroud,[60]

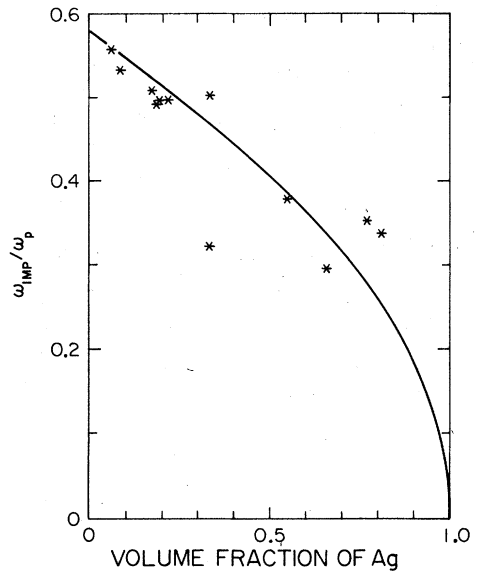

FIG. 20. Center frequency of the impurity band divided by plasma frequency vs volume fraction. The line is the expected result.

$$\omega_{\text{imp}} = \left[\frac{1-f}{3}\right]^{1/2} \omega_p \ . \tag{17}$$

The fit of the data to the theory is remarkably good. We see that the impurity band decreases in frequency with increasing volume fraction.

In summary, we have measured the optical properties of an Ag-KCl composite system and compared these properties with the theories for the effective dielectric function of an inhomogeneous medium. Our system is in qualitative agreement with most of the features of the EMA. The optical sum rules are obeyed for most of our samples. Finally, we have found that the "impurity band" does exist in our system and the concentration dependence of the band center agrees well with theory.

ACKNOWLEDGMENTS

We thank D. Stroud for numerous useful discussions and S. Miller and B. Farrar for assistance with the electron microscopes. This work was supported by the U.S. Department of Energy under Contract No. DE-AS02-78ER04914.

*Present address: AT&T Bell Laboratories, Bell Telephone Laboratories, Incorporated, Murray Hill, NJ 07974.

†Present address: Department of Physics, University of Florida, Gainesville, FL 32611.

[1]W. T. Doyle, Phys. Rev. **111**, 1067 (1958).

[2]R. H. Doremus, J. Chem. Phys. **40**, 2389 (1964).

[3]U. Kreibig and C. V. Fragstein, Z. Phys. **224**, 307 (1969).

[4]S. C. Jain and N. D. Arora, Solid State Commun. **15**, 433 (1974); **16**, 421 (1975).

[5]J. D. Ganiere, R. Rechsteiner, and M. S. Smithard, Solid State Commun. **16**, 113 (1975).

[6]R. S. Sennett and C. D. Scott, J. Opt. Soc. Am. **40**, 203 (1950).

[7]G. Rassigini and P. Rouard, J. Opt. Soc. Am. **53**, 604 (1963).

[8]R. H. Doremus, J. Appl. Phys. **37**, 2775 (1966).

[9]J. P. Marton, J. Appl. Phys. **40**, 5383 (1969).

[10]S. Yoshida, T. Yamaguchi, and A. Kinbara, J. Opt. Soc. Am. **61**, 62 (1971).

[11]R. W. Tokarsky and J. P. Marton, J. Appl. Phys. **45**, 3051 (1974).

[12]R. E. Hetrick and J. Lambe, Phys. Rev. B **11**, 1273 (1975).

[13]V. V. Troung and G. D. Scott, J. Opt. Soc. Am. **66**, 124 (1976).

[14]S. Norrman, T. Andersson, C. G. Granqvist, and O. Hunderi, Solid State Commun. **23**, 261 (1977); Phys. Rev. B **18**, 674 (1978).

[15]R. W. Cohen, G. D. Cody, M. D. Coutts, and B. Abeles, Phys. Rev. B **8**, 3689 (1973).

[16]E. B. Priestley, B. Abeles, and R. W. Cohen, Phys. Rev. B **12**, 2121 (1975).

[17]B. Abeles, H. L. Pinch, and J. I. Gittleman, Phys. Rev. Lett. **35**, 247 (1975).

[18]B. Abeles and J. I. Gittleman, Appl. Opt. **15**, 2328 (1976).

[19]J. I. Gittleman and B. Abeles, Phys. Rev. B **15**, 3273 (1977).

[20]P. Sheng, Phys. Rev. Lett. **45**, 60 (1980).

[21]G. A. N. Klasson, C. G. Granqvist, and O. Hunderi, Appl. Opt. **20**, 26 (1981).

[22]L. Harris and J. K. Beasley, J. Opt. Soc. Am. **42**, 134 (1952).

[23]D. R. McKenzie, J. Opt. Soc. Am. **66**, 249 (1976).

[24]C. G. Granqvist and O. Hunderi, Solid State Commun. **19**, 939 (1976).

[25]C. G. Granqvist, N. Calander, and O. Hunderi, Solid State Commun. **31**, 249 (1979).

[26]C. G. Granqvist and R. A. Buhrman, J. Appl. Phys. **47**, 2200 (1976).

[27]D. M. Grannan, J. C. Garland, and D. B. Tanner, Phys. Rev. Lett. **46**, 375 (1981).

[28]Evidence for this good contact comes from resistance studies where ordinary metallic behavior (no thermal activation) was seen from 300 to 0.002 K. See Ref. 27 and J. C. Garland, W. J. Gully, and D. B. Tanner, Phys. Rev. B **22**, 507 (1980).

[29]The darker area in Fig. 3 is where KCl has been dissolved from the surface and redeposited in a thin film over the sample. Microprobe x-ray analysis shows that the Ag particles have the same concentration in this region.

[30]H. Scher and R. Zallen, J. Chem. Phys. **53**, 3759 (1980).

[31]I. Webman, J. Jortner, and M. Cohen, Phys. Rev. B **11**, 2885 (1975).

[32]B. Warner (unpublished).

[33]K. D. Cummings, D. B. Tanner, and J. S. Miller, Phys. Rev. B **24**, 4142 (1981).

[34]R. B. Sanderson and H. E. Scott, Appl. Opt. **10**, 1097 (1971).

[35]H. Ehrenreich and H. R. Philipp, Phys. Rev. **128**, 1622 (1962).

[36]T. Huen, G. B. Irani, and F. Wooten, Appl. Opt. **10**, 552 (1971).

[37]K. W. Johnson and E. E. Bell, Phys. Rev. **187**, 1044 (1969).

[38]F. Wooten, *Optical Properties of Solids* (Academic, New York, 1972).

[39]C. Kittel, *Introduction to Solid State Physics,* 5th ed. (Wiley, New York, 1976).

[40]H. J. Hagemann, W. Gudat, and C. Kunz, Deutsches

Elektronen-Synchrotron, Hamburg, West Germany, Report No. DESY SR-7417, 1974 (unpublished).
[41]E. Simanek, Phys. Rev. Lett. **38**, 1161 (1977).
[42]For a review of the history of the field see R. Landauer, *Electrical Transport and Optical Properties of Inhomgeneous Media,* edited by J. C. Garland and D. B. Tanner (AIP, New York, 1978), p. 1.
[43]J. C. M. Garnett, Phil. Trans. R. Soc. London, Ser. A **203**, 385 (1904); **205**, 237 (1906).
[44]V. K. S. Shante and S. Kirkpatrick, Adv. Phys. **20**, 325 (1971).
[45]H. L. Scott, Jr., Am. J. Phys. **40**, 1134 (1972).
[46]D. M. Wood and N. W. Ashcroft, Philos. Mag. **35**, 269 (1977).
[47]D. J. Bergman, Phys. Rep. **43**, 377 (1978).
[48]G. L. Carr, R. L. Henry, N. E. Russell, J. C. Garland, and D. B. Tanner, Phys. Rev. B **24**, 777 (1981).
[49]D. A. G. Bruggeman, Ann. Phys. (Leipzig) **24**, 636 (1935).
[50]R. Landauer, J. Appl. Phys. **23**, 779 (1952).
[51]D. Stroud, Phys. Rev. B **12**, 3368 (1975).
[52]I. Webman, J. Jortner, and M. H. Cohen, Phys. Rev. B **15**, 5712 (1977); **16**, 2539 (1977).
[53]D. Stroud and F. P. Pan, Phys. Rev. B **17**, 1602 (1978).
[54]N. E. Russell, J. C. Garland, and D. B. Tanner, Phys. Rev. B **23**, 632 (1981).
[55]D. B. Tanner, A. J. Sievers, and R. A. Buhrman, Phys. Rev. B **11**, 1330 (1975).
[56]H. J. Trodahl, Phys. Rev. B **19**, 1316 (1979).
[57]L. Genzel and U. Kreibig, Z. Physik B **37**, 93 (1980).
[58]P. N. Sen and D. B. Tanner, Phys. Rev. B **26**, 3582 (1982).
[59]C. G. Granqvist, R. A. Buhrman, J. Wyns, and A. J. Sievers, Phys. Rev. Lett. **37**, 625 (1976).
[60]D. Stroud, Phys. Rev. B **19**, 1783 (1979).